Article

Cell Reports

Targeting Tumor Mitochondrial Metabolism Overcomes Resistance to Antiangiogenics

Graphical Abstract

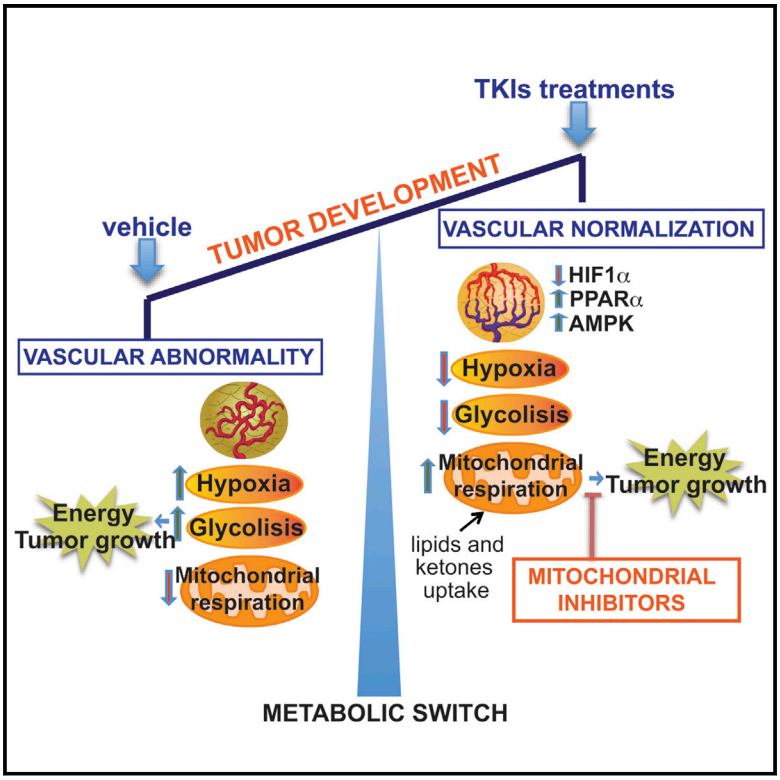

Authors

Paloma Navarro, Maria J. Bueno, Ivana Zagorac, ..., Francisca Mulero, Navdeep S. Chandel, Miguel Quintela-Fandino

Correspondence

mquintela@cnio.es

In Brief

Navarro et al. show that tumors treated with antiangiogenics can correct hypoxia and downregulate aerobic glycolysis. Tumors show metabolic plasticity, switching to mitochondrial metabolism, mediated by AMPK, PKA, and PPARα. Despite the adaptation, mitochondrial metabolism becomes essential for tumor survival. Thus, anti-mitochondrial agents induce metabolic synthetic lethality in this situation.

Highlights

- Anti-angiogenics can correct hypoxia in breast and lung tumors
- Normoxic tumors shut down glycolysis and rely on mitochondrial metabolism
- Mitochondrial metabolism is essential for tumor survival when normoxic
- Targeting mitochondrial metabolism is synergistic with antiangiogenics

Accession Numbers

GSE80778
PXD004071

Navarro et al., 2016, Cell Reports *15*, 2705–2718
June 21, 2016
http://dx.doi.org/10.1016/j.celrep.2016.05.052

Cell Reports
Article

Targeting Tumor Mitochondrial Metabolism Overcomes Resistance to Antiangiogenics

Paloma Navarro,[1,6] Maria J. Bueno,[1,6] Ivana Zagorac,[1] Tamara Mondejar,[1] Jesus Sanchez,[1] Silvana Mourón,[1] Javier Muñoz,[2] Gonzalo Gómez-López,[3] Veronica Jimenez-Renard,[1] Francisca Mulero,[4] Navdeep S. Chandel,[5] and Miguel Quintela-Fandino[1,*]
[1]Breast Cancer Clinical Research Unit
[2]Proteomics Unit
[3]Bioinformatics Unit
[4]Molecular Imaging Unit
CNIO–Spanish National Cancer Research Center, Melchor Fernández Almagro, 3, 28029 Madrid, Spain
[5]Division of Pulmonary and Critical Care Medicine, Department of Medicine, Feinberg School of Medicine, Northwestern University, Chicago, IL 60611, USA
[6]Co-first author
*Correspondence: mquintela@cnio.es
http://dx.doi.org/10.1016/j.celrep.2016.05.052

SUMMARY

Epithelial malignancies are effectively treated by antiangiogenics; however, acquired resistance is a major problem in cancer therapeutics. Epithelial tumors commonly have mutations in the MAPK/Pi3K-AKT pathways, which leads to high-rate aerobic glycolysis. Here, we show how multikinase inhibitor antiangiogenics (TKIs) induce hypoxia correction in spontaneous breast and lung tumor models. When this happens, the tumors downregulate glycolysis and switch to long-term reliance on mitochondrial respiration. A transcriptomic, metabolomic, and phosphoproteomic study revealed that this metabolic switch is mediated by downregulation of HIF1α and AKT and upregulation of AMPK, allowing uptake and degradation of fatty acids and ketone bodies. The switch renders mitochondrial respiration necessary for tumor survival. Agents like phenformin or ME344 induce synergistic tumor control when combined with TKIs, leading to metabolic synthetic lethality. Our study uncovers mechanistic insights in the process of tumor resistance to TKIs and may have clinical applicability.

INTRODUCTION

Epithelial tumors commonly harbor oncogenic alterations in the MAPK and Pi3K-AKT axes (Kandoth et al., 2013). These pathways drive aerobic glycolysis, the main source of energy and uptake of "building blocks" for tumor growth (Foster et al., 2012; Garcia-Cao et al., 2012; Lunt and Vander Heiden, 2011; Ying et al., 2012). Pathologic tumor angiogenesis, which is linked to interstitial hypoxia, supports enhanced glycolysis (Jain, 2005; Ostergaard et al., 2013). Extensive work by Rakesh Jain and Robert Kerbel shows that, at least in some cases, antiangiogenic agents may elicit their effect by reversting the abnormal physiology of tumor blood vessels (caused by a disequilibrium between pro- and antiangiogenic factors), normalizing tumor oxygenation, and correcting other features that support tumor progression (Jain, 2005, 2013; Kerbel, 2006). Acquired resistance to antiangiogenics is a major problem in cancer therapeutics, since antiangigoenic agents are the most widely used biologic agents in oncology and are approved by the Food and Drug Administration (FDA) for use against breast, colorectal, lung, ovarian, kidney, and liver cancer, among other malignancies. Several resistance mechanisms, mainly involving specific compensatory signaling loops, have been described and have potential clinical impact due to newly developed compounds that target them (Lu et al., 2012; Oliner et al., 2004). However, the effects of the pharmacologic modulation of multiple kinases, plus the alteration of oxygen and nutrient levels secondary to the disruption of blood vessel homeostasis, may induce pleiotropic adaptive responses involving several pathways intertwined across multiple -omic levels. We hypothesize that, in cases in which antiangiogenics lead to hypoxia normalization, chronic high-rate glycolysis is offset and tumors might switch to an alternative metabolic source. If this alternative source were essential for tumor survival, it would open up therapeutic opportunities.

Two main types of antiangiogenics have been developed: monoclonal antibodies (mAbs) and multi-tyrosine-kinase inhibitors (TKIs). Among the TKIs, sorafenib and sunitinib have been tested the most extensively in phase III trials, but, aside from liver/kidney cancers, their therapeutic effects have not been positive. Both drugs yielded negative phase III trials in lung (Heist et al., 2014; Scagliotti et al., 2010) and breast cancer (Baselga et al., 2013; Crown et al., 2013). Nintedanib is a recently developed TKI that has recently been approved based on a positive trial in lung cancer (Reck et al., 2014). Promising results have also been observed in breast cancer (Quintela-Fandino et al., 2014). Nintedanib and dovitinib, another TKI with a very similar profile, differ from older TKIs by having lower K_M values against pro-angiogenic kinases. Theoretically, TKIs, since they act over

several angiogenic axes, could be more likely to reverse the abnormal balance between the plethora of pro- and antiangiogenic factors that cause tumor vascular abnormality (Jain, 2005, 2013) compared with agents that target a single pro-angiogenic factor. Several TKIs are under active development for many malignancies. Thus, it is important to address the mechanisms of acquired resistance against TKIs.

This study explores the mechanism of adaptation against recently developed antiangiogenic TKIs in the realm of cancer metabolism and the potential synthetic-lethal therapeutic implications that result. The effects of several TKIs (nintedanib and dovitinib, and external validation of the findings with regorafenib) are examined in breast and lung cancer models (genetically engineered mouse models of cancer and tumor xenografts).

RESULTS

TKIs Oxygenate the Interstitium and Downregulate Glucose Uptake while Inhibiting Tumor Growth

The PyMT breast cancer model was backcrossed to a pure Friend virus B (FVB) background for ten generations, creating a spontaneous breast cancer model with the characteristics depicted in Figure S1 (hormone-receptor positive, high replicative fraction, and sensitive to tamoxifen), and which recapitulates the phenotype of approximately one-third of the hormone-receptor positive tumors seen in the clinics. In this model, invasive lesions were present at 4 weeks of age (Figure S1), and tumors reached an average size of 100 mm^3 at approximately 7 weeks of age. The PyMT oncogene activates the MAPK and Pi3K-AKT pathways (Figure S2A). This activation leads to high glucose uptake (Figure S2B), which makes it a good model to study the effects of TKIs in the Warburg effect.

Starting at 7 weeks of age (T_0) we exposed mice to long-term treatment with vehicle, nintedanib, or dovitinib. We used B20-4.1.1 as the reference antiangiogenic agent. B20-4.1.1 is a mAb with activity against human and murine VEGF that substituted for bevacizumab in preclinical research in mice (Liang et al., 2006). The animals were treated on a continuous schedule, as in a clinical setting. The adaptive changes occurring during treatment were monitored along a time course: T_0, T_1 (week 1 of treatment), and T_{end}. The efficacy parameter under study was tumor growth inhibition (TGI) at the time when vehicle-treated animals reached the humane euthanization endpoint (T_{end}).

The two TKIs block human and murine VEGFR, PDGFR, and FGFR families with similar K_M values. To avoid the potential confounding effects of FGFR1 blockade (a kinase implicated in driving oncogenic addiction in 10% of breast cancers; Curtis et al., 2012), the absence of FGFR1 expression in this model was confirmed (Figure S1F).

Rapidly growing tumors are supported by abnormal vessels (Jain, 2005), leading to hypoxia that triggers the transcriptional program that fuels the Warburg effect (Jain, 2005; Ostergaard et al., 2013). Both the TKIs and the reference antiangiogenic agent B20-4.1.1 caused ~60% TGI (Figure 1A) and affected microvessel density in a similar manner (Figure 1B). However, the TKIs normalized the vasculature (Figure 1C) and thus intratumor hypoxia (Figure 1D). In comparison, tumors treated with B20-4.1.1 or vehicle showed progressively increased hypoxia and vessel abnormality. Congruently with the decrease in hypoxia, the TKI-treated tumors showed decreased glucose uptake (measured with 18F-FDG-PET ([^{18}F]fluorodeoxyglucose [FDG] micro positron emission tomography [PET]) during treatment compared to tumors treated with vehicle (Figure 1E). Treatment with B20-4.1.1 did not normalize the vasculature or hypoxia, and glucose avidity was subsequently maintained similar to that for untreated tumors (Figures 1C–1E).

Tumors that Become Normoxic Because of Exposure to TKIs Switch to Mitochondrial Metabolism

Rapidly growing tumors increase aerobic glycolysis (i.e., Warburg effect) due to oncogenic and tumor suppressor mutations, resulting in tumor uptake of glucose to support biosynthesis of macromolecules required for cell proliferation, which is further supported by tumor hypoxia (Foster et al., 2012; Garcia-Cao et al., 2012; Lunt and Vander Heiden, 2011; Ying et al., 2012). Among the differences observed at the microenvironmental level, how tumors with hyperactive PI3K/AKT and MAPK were able to continue growing despite lack of hypoxia development and a 2-fold decrease in glucose uptake under TKI treatment was most interesting. The potential of tumor metabolism reprogramming in animals treated with nintedanib was investigated, using vehicle as a control and B20-4.1.1 as a reference antiangiogenic. In subsequent experiments, B20-4.1.1-treated tumors behaved like vehicle-treated tumors; data are not shown unless required for experimental data layout, because the adaptive changes regarding resistance to mAb antiangiogenic treatment have been described elsewhere (Chung et al., 2013; Xu et al., 2014).

We studied more than 320 metabolites and 40 metabolic routes in 109 tumors in a gas chromatography/liquid chromatography (GC/LC)-mass spectrometry (MS)-guided metabolomic study. Tumor glucose concentration decreased over time in both treatment groups; however, glycolysis metabolites like glucose-6-phosphate and lactate were diminished in nintedanib-treated tumors compared to vehicle (Figure 2A). Although steady-state determinations do not allow inference of true metabolic fluxes, these data suggest decreased glycolytic use of glucose. Another feature of aerobic glycolysis is the fueling of the pentose-phosphate shunt from glucose-6-P for biosynthetic purposes (Lunt and Vander Heiden, 2011). End products of the oxidative (ribulose) and nonoxidative phases (sedoheptulose-7-phosphate, ribose-5-phosphate [R-5P], xylulose-5-phosphate [X-5P]) of the pathway were also decreased in nintedanib-treated tumors (Figure 2B). Decreased glycolysis could be compensated by an increased mitochondrial tricarboxylic acid (TCA) cycle. TCA uses pyruvate, ketones, and carnitine-bound fatty acids as substrates. An almost 2-fold increase in intratumor 3-hydroxybutyrate and carnitine-bound end products of β-oxidation acetylcarnitine and butyrylcarnitine concentration were detected in tumors treated with nintedanib compared to those treated with vehicle (Figure 2C).

In healthy tissues, mitochondrial use of these nutrients increases during nutritional stress and is controlled by PPARα transcription factors, which enhance transcription of lipolytic and oxidative phosphorylation enzymes and induce fatty acid

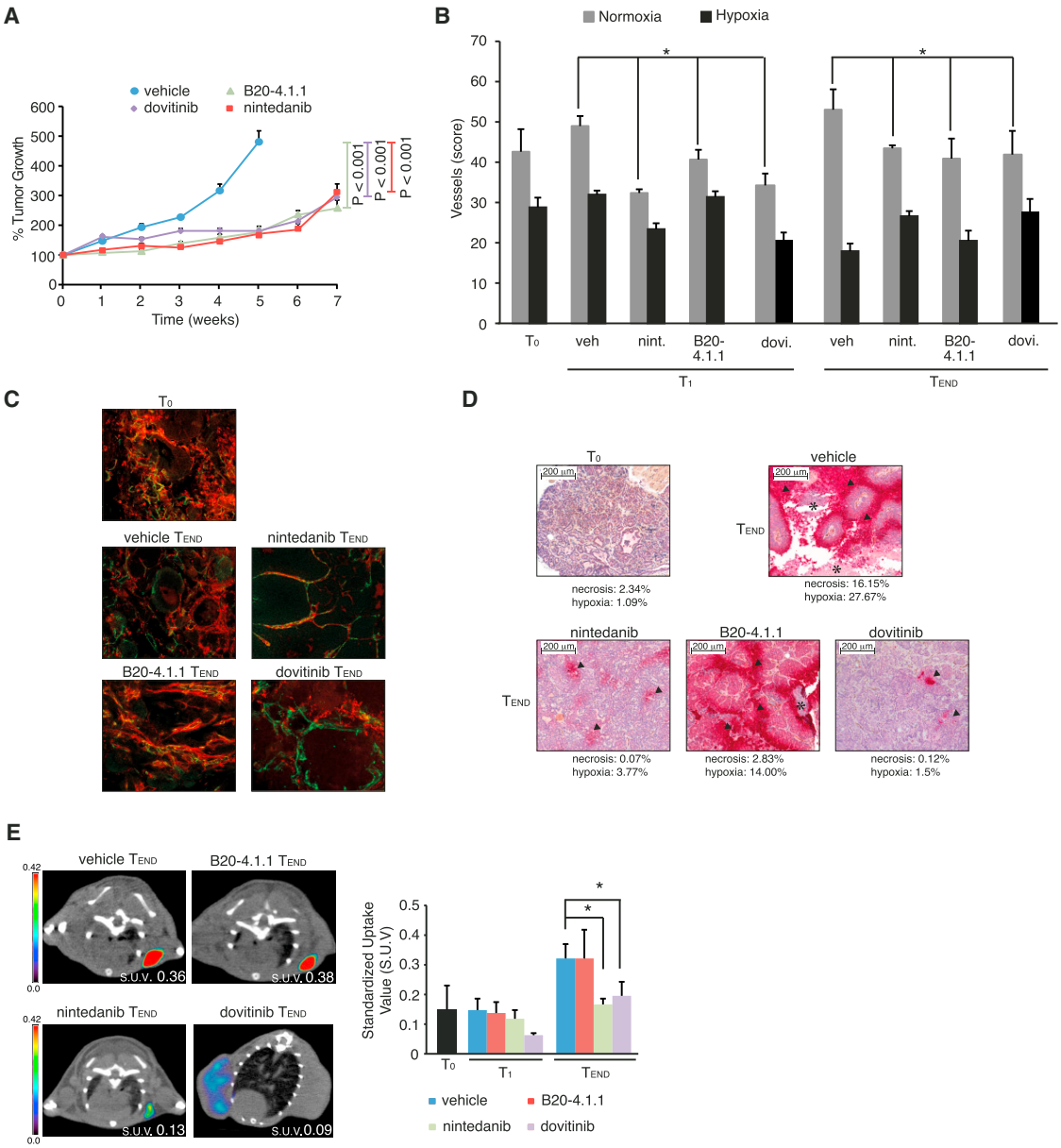

Figure 1. TKI Antiangiogenics Induce Normoxia and Decrease Tumor Glucose Avidity while Inhibiting Tumor Growth

(A) Tumor growth inhibition (TGI) exerted by nintedanib (64.6%), dovitinib (62.6%), or B20-4.1.1 (63.9%). n > 150 tumors per group.

(B) Microvessel density assessed both in the hypoxic (pimomidazole staining-positive) and normoxic (pimomidazole-negative) areas). The p value (t test) was significant (<0.05) for the three treatment groups versus vehicle at T_1 and T_{end} in the pimomidazole-negative areas.

(C) Decreased 10KD-dextran-FITC extravasation (red staining in the peri-vascular areas, evidenced by anti-CD31 staining, green) and stasis in the tumor interstitium and vessel tortuosity, parameters that mirror vascular abnormality, were observed as TKI-treated tumors grew compared to vehicle.

(D) Progression of hypoxia (pimomidazole [dark-red] staining, arrowheads) and necrosis (asterisks) along the different treatments. The numbers represent the percentage of the tumor area stained by pimomidazole or with necrosis.

(E) Tumor glucose uptake by FDG-PET was significantly lower over the long term with nintedanib treatment (−20%, p = 0.22 at T_1; −48.5%, p < 0.001 at T_{end}) and dovitinib (−48%; p = 0.012 at T_1; −44%, p < 0.008 at T_{end}). n > 50 tumors per time point and group. Error bars, SEM.

oxidation: PKA, which is activated by B2 receptor stimulation and, in turn, activates the hormone-sensitive peripheral lipase; and AMPK activation, a kinase that upregulates aerobic degradation of nutrients (Soeters et al., 2012). A transcriptomic study suggested that the same mechanisms, directed to increase mitochondrial metabolism, were set in motion in nintedanib-treated tumors. A gene set enrichment analysis of the tumor transcriptome showed upregulation of aerobic catabolism pathways and PPAR signaling in nintedanib- versus vehicle-treated tumors (Figure 3A), supporting the enzymatic processes behind

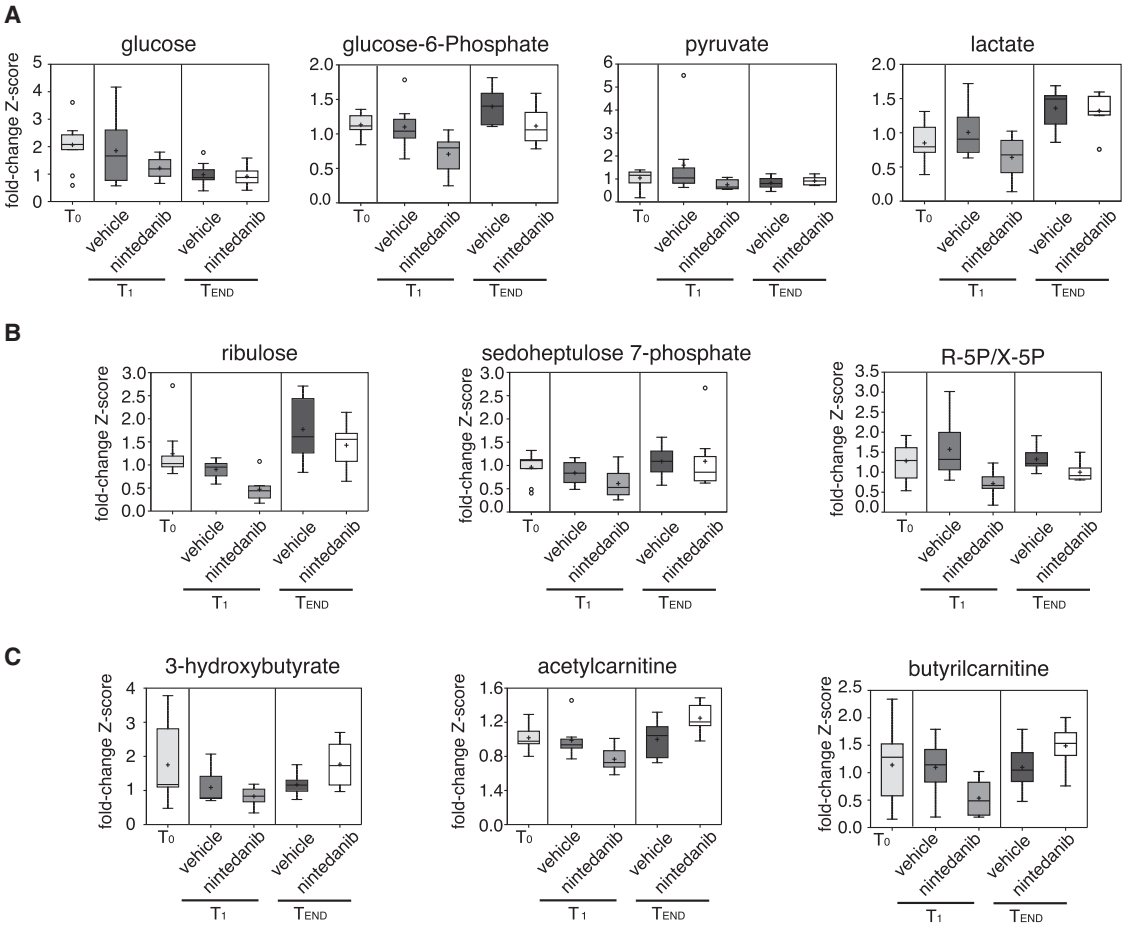

Figure 2. Downregulation of Glycolysis and Pentose-Phosphate Shunt and Increased Metabolites Targeted for Mitochondrial Degradation

The boxplots (A–C) represent the following: raw area counts for each species were log-transformed and rescaled to have a median equal to 1 (calculated from the acquisition spectra of 109 tumors). For each tumor, a ratio was calculated versus the median. Boxplots with the ratios of 14–16 tumors per time point and condition were plotted for each species. +, mean value; —, median value; o, extreme data point. Because of the asymmetric nature of the data distribution, median values are more representative than means.

(A) Glycolytic intermediates.

(B) Intermediates of the pentose-phosphate pathway. R-5P and X-5P are isomers and are in equilibrium, thus determined inseparably.

(C) Metabolites targeted for mitochondrial degradation and O_2-consumption-coupled ATP generation.

the metabolic switch. To increase robustness, we examined whether congruent signalosome changes occurred. A MS-based phosphoproteomic assay was conducted using isobaric tagging and approximately 1,000 phospho-peptides were identified. Using MaxQuant, the putative kinases responsible for the phosphorylation of each residue identified were predicted. Examination of the clustering of the phosphorylation status of AMPK1/2 and PKA substrates into random or real patterns suggested that the activity of both was increased with nintedanib treatment (Figure 3B). Eighteen phosphorylated AMPK1/2 substrates were identified, eight of which showed increased phosphorylation at T_{end} in nintedanib-treated animals compared to tumors treated with either vehicle or B20-4.1.1 (Figure 3B, left panel; Table S1; B20-4.1.1 data are shown as the generation of hypothetical random clusters considered three-way patterns). Eleven of those 18 substrates showed increased phosphorylation from T_0 to T_1 to T_{end} with nintedanib treatment (Figure 3B, middle panel, and Table S2). In addition, 288 of 590 identified PKA substrates showed increasing phosphorylation from T_0 to T_1 to T_{end} with nintedanib treatment (Table S3). Among the AMPK- and PKA-regulated substrates, the hydroxypyruvate reductase Glyr1, which is known to promote β-oxidation in plants (Pracharoenwattana et al., 2010), and IRS-1 (serine/threonine phosphorylation antagonizes the insulin-induced tyrosine-phosphorylation events involved in glucose uptake and anabolic pathways [Li et al., 2008]) were identified, respectively.

Taken together, the presented data suggest that tumor metabolism was reprogrammed in response to TKIs, with mitochondrial metabolism increasing under the control of PPAR-α, AMPK, and PKA activation in response to decreased glycolysis. We focused on finding further mechanistic proof of the metabolic switch and on demonstrating that TKIs induced increased mitochondrial respiration, by conducting a mechanistic validation study with both agents.

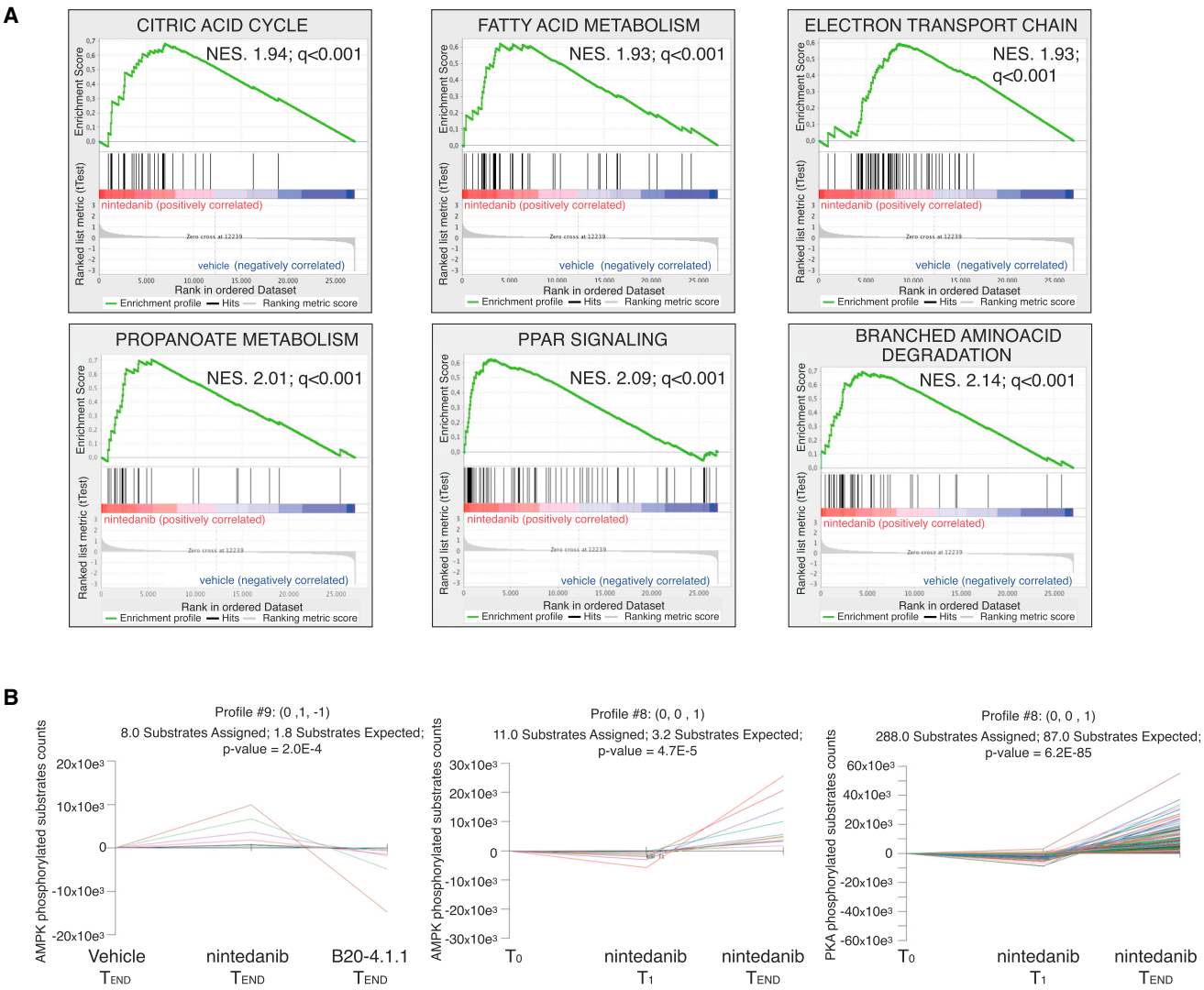

Figure 3. Reprogramming at the Transcriptomic and Phosphoproteomic Levels Supports the Metabolic Switch

(A) Gene enrichment analysis plots showing activation of pathways involved in aerobic metabolism in T_{end} of nintedanib- versus vehicle-treated tumors. NES, normalized enrichment score. The q value is the false discovery rate.

(B) Phosphorylation levels of predicted AMPK and PKA substrates.

As shown, TKIs prevented the development of hypoxia. HIF1α is the main controller of the response to hypoxia, and the inhibition of mitochondrial respiration and upregulation of glycolysis are two of its main downstream effects. Vehicle-treated tumors showed increased HIF1α levels with tumor progression, but HIF1α was undetectable in TKI-treated tumors of the same size (Figure 4A). The PyMT oncogene downregulates the function of phosphatases at the Pi3K/AKT and MAPK levels, which is associated with high glucose avidity. Thus, resilient activation of both pathways, despite the environmental conditions, would be expected. Such was the case for phospho-ERK (Figure 4B). However, congruent with the phosphorylated IRS-1 residue identified by MS and implicated in downregulating insulin-driven IGF-1R signaling, AKT phosphorylation was decreased in TKI-treated tumors (Figure 4C). The ATP sensor AMPK requires ser-172 phosphorylation for activation of its downstream cascade leading to downregulation of glycolysis and upregulation of mitochondrial metabolism. Consistent elevation of p-AMPK was observed in both TKI-treated tumors (Figure 4D) (these tumors were LKB1-positive; Figure 4E). Phospho-CREB, a substrate that translates PKA activity, showed increased phosphorylation in TKI-treated tumors (Figure 4F). In addition, the transcription factor PPARα was also upregulated in TKI-treated tumors (Figure 4G). The immunohistochemistry data shown in Figure S3A show that the observed changes occur in the tumor-epithelial compartment.

Taken together, the presented data suggest that under chronic treatment with antiangiogenic TKIs, tumors remain normoxic, which abrogates HIF1α stabilization. The lack of HIF1α together with the decreased AKT signaling contributes

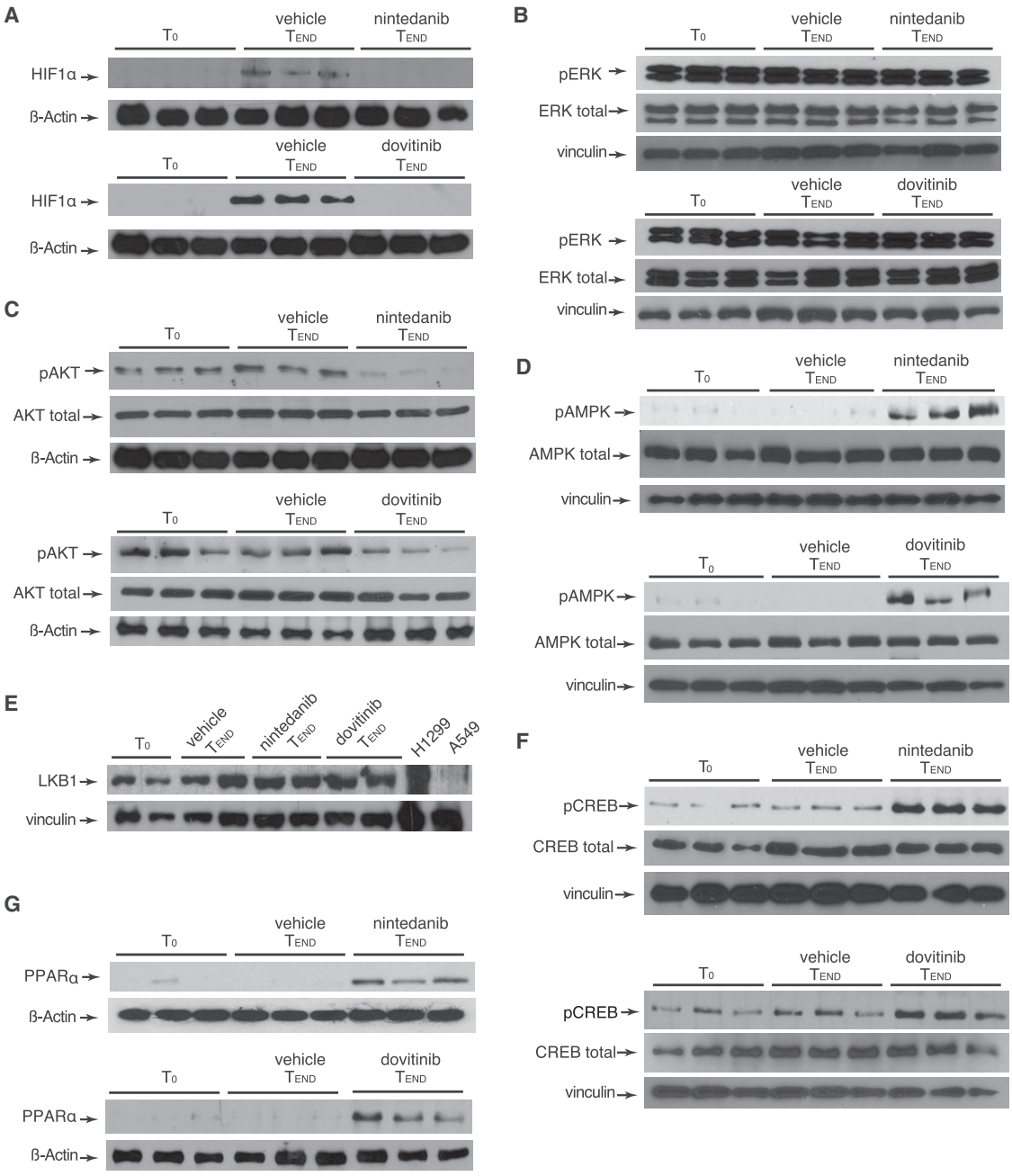

Figure 4. Signaling Changes Accounting for Decreased Glycolysis and Increased Mitochondrial Metabolism during the Adaptive Response against TKIs

Immunoblots of lysates from tumors dissected at T_{end} from mice chronically treated with vehicle, dovitinib, or nintedanib. Tumors were obtained from the upper mammary glands from three different animals per condition.

(A) HIF1α staining.

(B) pERK and total ERK staining.

(C) pAKT and total AKT staining.

(D) pAMPK and total AMPK staining.

(E) LKB1 staining; a positive and a negative control lysate were included for LKB1.

(F) pCREB and total CREB staining.

(G) PPARα staining. Actin or vinculin were used as loading controls depending on the molecular weight of the probes.

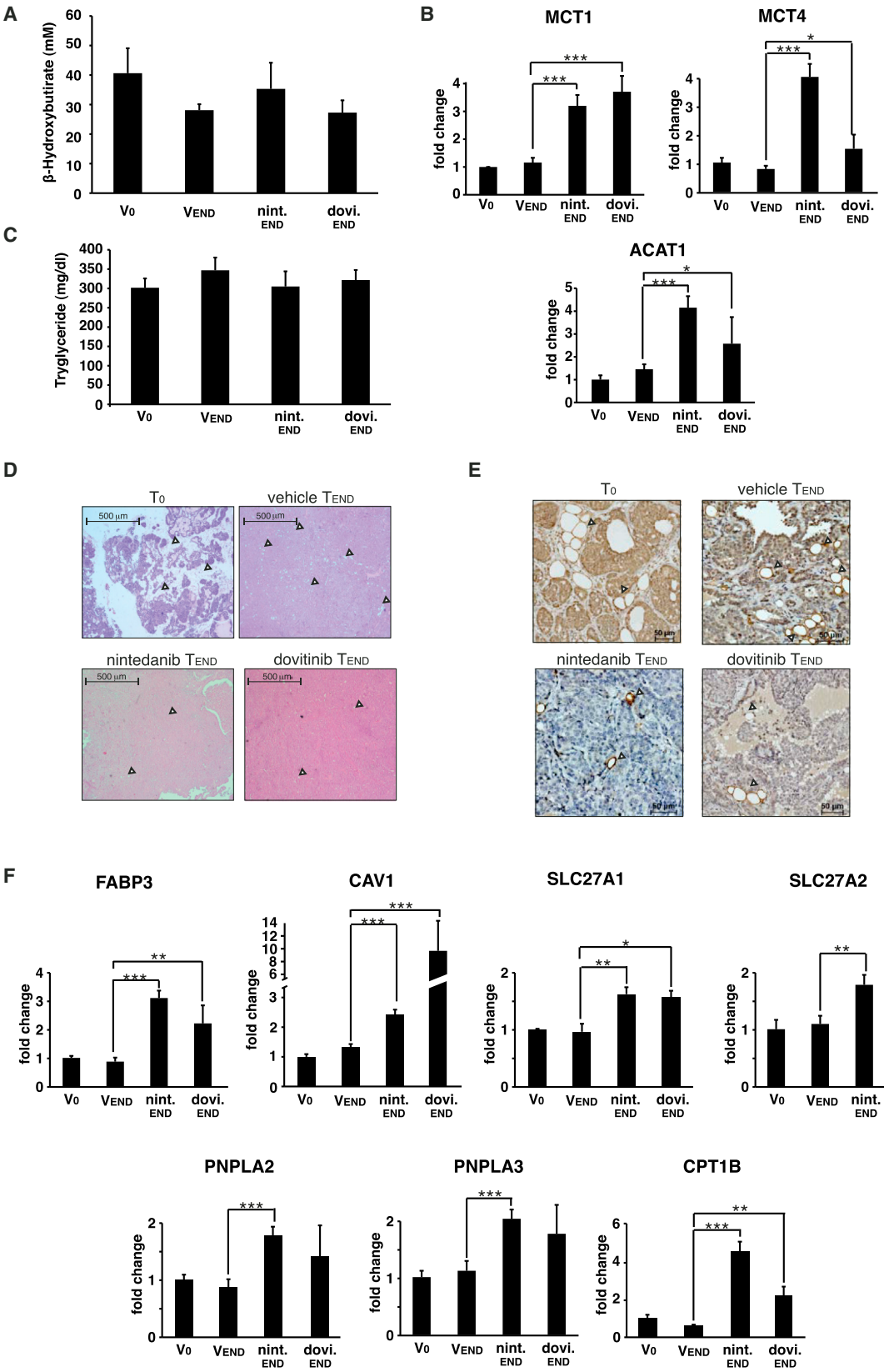

(legend on next page)

to the decreased glycolysis output. This leads to relative nutritional stress, evidenced by AMPK, PKA, and PPAR-α activation. The -omic determinations suggest increased mitochondrial metabolism, which could compensate for this tumor nutritional stress. Thus, we sought to determine the source of nutrients for mitochondrial metabolism (elevated concentration of fatty acids and ketones found in tumors by MS) and to prove the increased mitochondrial respiration in vivo in this system.

Ketone bodies are synthesized in the liver, and, unless an individual undergoes nutritional starvation, baseline production remains stable and blood levels barely change (Soeters et al., 2012). Expression of the enzymatic machinery accounting for ketone synthesis in tumors was not observed (data not shown). Blood ketone levels remained stable over time (Figure 5A); however, a >2.5-fold upregulation of the ketone-body transporters MCT1 and four in TKI-treated tumors was detected, compared to vehicle-treated tumors, coupled with a >4-fold increase in the levels of ACAT1, the enzyme that allows re-use of ketone bodies as mitochondrial substrates (Figure 5B). These observations suggest active uptake of ketones from the background pool synthesized in the liver and released to the bloodstream. Because of the relative small contribution of the tumor compartment to body weight (less than approximately 1/30 at T_{end}), the tumor-restricted starvation was probably not sufficient to produce systemic ketosis and cause blood level fluctuations of these species.

Regarding fatty acids, plasma triglycerides were measured and no differences were found among the treatment groups (Figure 5C). However, tumor histologic analysis revealed a differential pattern for lipidic deposits (hematoxylin/eosin, Figure 5D; or perilipin staining, Figure 5E) between TKI- or vehicle-treated tumors. Throughout the treatment time, adipose deposits remained stable (10%–15% of the tumor section) in vehicle-treated tumors, whereas they almost disappeared with TKI treatment. In addition, increased levels of the fatty acid transporters FABP3, CAV1, and SLC27A1/A2 and the lipases PNPLA2 and 3 were found in tumors (Figure 5F), coupled with an ~4-fold upregulation of CPT1B (Figure 5F), which shuttles the carnitine-bound species committed for mitochondrial degradation into the mitochondrial matrix. Taken together, these data suggest that the tumor cells took up fatty acids from the surrounding adipocytes. The immunohistochemistry showed in Figure S3B show that the upregulation of ketone bodies and fatty acids transporters and enzymes implicated in their degradation occurred in the tumor epithelial compartment.

In an attempt to demonstrate increased mitochondrial metabolism in tumors, an enzymohistochemical assay was performed to measure respiratory activity on fresh tissue (Taylor et al., 2003). Succinate dehydrogenase (SDH) or complex II is an enzyme complex bound to the inner mitochondrial membrane that catalyzes the eighth step of the Krebs cycle (oxidation of succinate to fumarate), while reducing ubiquinone to ubiquinol (second step of electron-transport chain). The reaction translates to increased aerobic activity (dark blue versus light or no staining). The assay, performed in fresh tumors right after sacrifice at T_1 and T_{end}, showed increased mitochondrial metabolism with either TKI, even at early time points (Figure 6A). Of note, TKI-treated tumor tissue had more intense staining than striated muscle fibers that were included in the histologic preparations as positive control and were located adjacent to the breast tumors.

We measured the oxygen consumption rate of cells freshly extracted from tumors treated until T_{end} with either vehicle or TKI, using the Seahorse Mito-Stress test. In both cases (Figures 6B and 6C), the coupled respiratory capacity was ~2-fold higher in tumors treated with TKI versus vehicle. Phenformin, a biguanide that blocks mitochondrial respiration through inhibition of complex I (El-Mir et al., 2000), suppressed mitochondrial respiration at 1,000 nM (Figure 6B).

The Switch to Mitochondrial Metabolism Is Necessary for Tumor Survival: Metabolic Synthetic Lethality

If the increased mitochondrial metabolism was relevant as an energy source in the context of TKI treatment, then the pharmacologic modulation of mitochondrial respiration might be ineffective if used as monotherapy. However, it should enhance the effects of the TKIs. We sought to prove the pro-survival role of mitochondrial metabolism during the adaptive tumor response to chronic treatment with TKI antiangiogenics.

Tumors were treated for 4 weeks with nintedanib and then the animals were exposed to a short course (3 days) of vehicle or phenformin. The administered dosage (300 mg/kg per day) of phenformin was observed to reverse the "mitochondrial phenotype" induced by nintedanib treatment (Figure 6D). Knowing that phenformin was able to induce the expected pharmacodynamic effects, the TGI properties of the various combinations predicted by our model were tested. Phenformin, despite pharmacodynamic proof of activity (suppression of respiration ex vivo [Figure 6B] and in vivo [Figure 6D]), was not effective when administered in monotherapy (17% TGI; $p = 0.88$). However, phenformin had a synergistic effect with nintedanib (TGI increased from 64% to 86%, $p = 0.004$). The addition of phenformin to dovitinib was synergistic as well, increasing the TGI from 62% to 82% ($p = 0.003$), suggesting TKI-induced tumor

Figure 5. Increased Ketone Bodies and Fatty Acids Transporters and Shuttles for Mitochondrial Degradation, Coupled with Decreased Adipose Deposits, in Tumors from TKI-Treated Animals

(A and C) Plasmatic levels of ketones and fatty acids did not significantly differ between vehicle- and TKI-treated animals.

(B) qRT-PCR values of MCT1, MCT4, and ACAT1 normalized to T_0 tumors. Asterisks were used for indicating significant differences between samples: *$p < 0.05$, **$p < 0.001$, ***$p < 0.0001$.

(D) H&E staining revealed a solid histologic pattern, with scarce adipose (arrowheads) deposits in TKI-treated tumors versus untreated.

(E) Immunohistochemistry (IHC) staining of perilipin confirmed a decrease (13.8% of tumor surface area to 2.6%; $p = 0.012$) in fat depots (arrowheads) with time in TKI-treated tumors. The intracellular (epithelial) lipid droplets also decrease with nintedanib/dovitinib treatment compared to vehicle-treated tumors.

(F) qRT-PCR of fatty acid transporters, lipases, and mitochondrial shuttle in vehicle- and TKI-treated animals. Asterisks were used for indicating significant differences between samples: *$p < 0.05$, **$p < 0.001$, ***$p < 0.0001$.

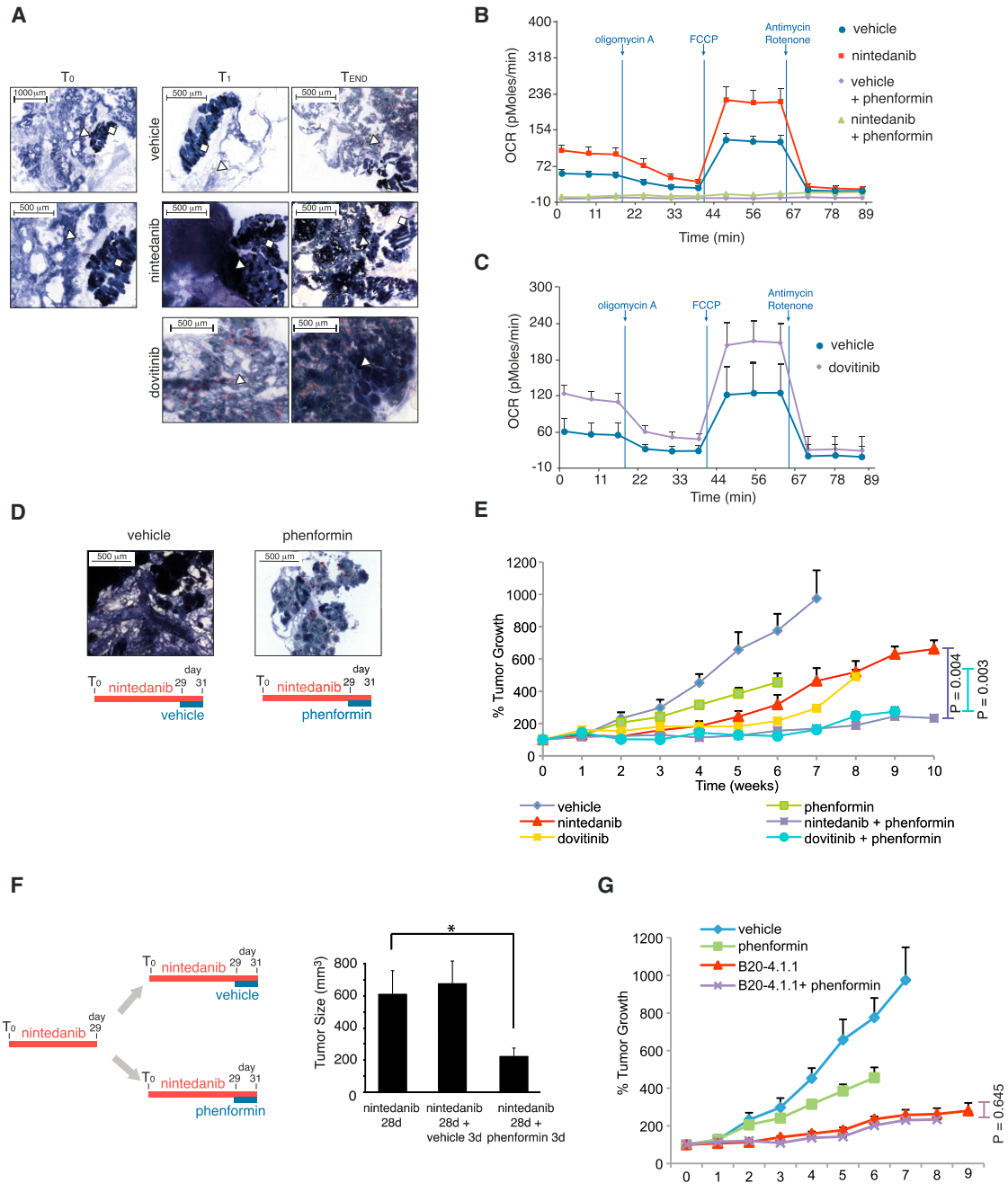

Figure 6. Evidence of Continuous, Long-Term, Increased Mitochondrial Respiration In Vivo in Tumors Treated with TKIs and Metabolic Synthetic Lethality

(A) The SDH activity in tumor cells (arrowheads) or striated muscle (squares, included as positive controls) is shown. The increased activity in tumor cell was evident from 1 week of treatment and was maintained for more than 2 months.

(B and C) Oxygen-consumption rate from nintedanib- and dovitinib-treated tumors versus vehicle; respiration was suppressed by phenformin.

(D) In vivo pharmacodynamic effects of phenformin: animals treated for 4 weeks with nintedanib were then treated for 3 days with vehicle (left) or phenformin (right), showing a dramatic decrease of SDH activity in tumors in the latter case.

(E) Tumor growth inhibition with phenformin or either TKI alone or in combination. n > 50 tumors per group; error bars, SEM.

(F) Using the same treatment schedule as in (D), the 3-day course of phenformin was sufficient to induce an average 73% reduction in tumor size ($p = 0.012$), what we termed "metabolic synthetic lethality," whereas tumors from animals receiving a 3-day course of vehicle experienced a slight growth. The chart represents the average tumor size before and after 3 days of vehicle of phenformin (n = 12).

(legend continued on next page)

dependence on mitochondrial respiration (Figure 6E). These data suggest that although mitochondrial metabolism can be pharmacologically inhibited with phenformin, it is only necessary for tumor survival when glycolysis has been downregulated by chronic antiangiogenic TKI treatment.

In addition, tests were conducted to determine whether a sequential, rather than concurrent, schedule would have more intense therapeutic effects; that is, whether adding phenformin after the mitochondrial phenotype has been "induced" would be more effective. Dependence on mitochondrial metabolism was induced by priming the tumors with nintedanib treatment (4 weeks) and then exposing them to phenformin or vehicle for only 3 days. The therapeutic effects on established large tumors are shown in Figure 6F. This suggests that mitochondrial activity is essential for replacing the decrease in aerobic glycolysis and for allowing tumors to withstand prolonged treatment with anti-angiogenic TKIs. Other aerobic metabolism inhibitors (PPARα- and beta-blockers) increased the therapeutic effects of the TKIs (Figure S4) as well.

According to this model, phenformin should not be effective when added to the reference antiangiogenic treatment (B20-4.1.1), because it does not induce hypoxia correction. The combination lacked therapeutic effects (Figure 6G).

Finally, phenformin has been reported to directly influence endothelial cell survival (Orecchioni et al., 2015). It has also been shown that phenformin can modulate HIF1α and VEGF production (Hsu et al., 2013; Martin et al., 2012). Such effects could interfere with the observed metabolic synthetic lethality. According to our data, none of those effects were a major contributor to the observed therapeutic effects of the combinations (Figure S5). On the other hand, the observed metabolic response was not part of a TKI-induced tumor cell-autonomous response (Figure S6), since chronic treatment with TKIs did not induce changes in maximum oxygen consumption rate (Figure S6A), or AKT, HIF, AMPK, or PPAR-alpha levels (Figure S6B). In addition, chronic treatment with TKIs did not sensitize the BRL1468 cell line to phenformin in vitro, as opposed to the observed effects in vivo (Figure S6C).

The Therapeutic Synergy Is Observed with the TKI Regorafenib and the Mitochondrial Inhibitor ME344 and Can Be Extended to Other Cancer Models

The therapeutic effects of using a different mitochondrial inhibitor or an additional TKI were tested in the PyMT model. The results in Figure 7A show that when ME344, another clinical-grade mitochondrial inhibitor (Bendell et al., 2015) that lacked efficacy in monotherapy (TGI = 7.4%) is used instead of phenformin, the effects are also synergistic (nintedanib: 64%; nintedanib + ME344: 92%; $p < 0.05$). Regorafenib, a TKI recently approved for colorectal cancer, lacked efficacy in monotherapy. However, the combination with ME344 abrogated tumor growth (TGI increased from −4.5% to 88%; $p < 0.05$). ME344 induced similar effects to those of phenformin in mitochondrial respiration (Figures S7A and S7B), and the mechanisms by which regorafenib induced sensitivity to ME344 were similar to those observed for the remaining TKIs (Figures S7C–S7F).

In order to test the applicability of the observed phenomenon, the therapeutic tests were extended to include two lung cancer models because nintedanib has recently been approved by the FDA for the treatment of this disease on the basis of improved overall survival in a phase III trial (Reck et al., 2014).

Pulm24 is a lung-cancer-patient-derived xenograft (PDX). This PDX is an adenocarcinoma of the lung, mutant for KRAS and wild-type for EGFR. Nintedanib alone was able to significantly delay tumor growth (Figure 7B). Similar to the PyMT model, nintedanib caused a profound inhibition of glucose uptake measured by FDG-PET (Figure 7C). Phenformin alone did not show antitumor effect, but the combination of nintedanib plus phenformin abrogated tumor growth, as predicted by our hypothesis (Figure 7B).

The Lewis lung carcinoma (LLC) model is the most (primarily) resistant of the models commonly used for testing the activity of new drugs, especially those with antiangiogenic properties (Nisancioglu et al., 2010; Shojaei et al., 2007). This model was considered interesting for two reasons: first, because a significant percentage of patients have primary resistance to this drug class as well; and second, because albeit transplantable, it is a spontaneous cancer model. The LLC model grows extremely rapidly, causing local wounds and ulcerations at the heterotopic graft site. According to our Institutional Animal Welfare Committee rules, the animals have to be sacrificed at this point, and pictures from ulcerations cannot be shown. Thus, survival curves (determined by the ulceration-driven sacrifice dates) are more illustrative than tumor size growth curves. As expected, nintedanib alone lacked therapeutic effect (so did phenformin; Figure 7D). Nintedanib decreased glucose uptake as well (Figure 7E). As expected, phenformin added to nintedanib prolonged median overall survival by >40% (log-rank $p < 0.001$; Figure 7D).

DISCUSSION

These findings link acquired resistance to a powerful anticancer drug class with aberrant cancer metabolism. The data show that under selective pressure tumor plasticity allows sustained tumor growth over the long term despite exposure to antiangiogenic TKIs, but it renders mitochondrial metabolism necessary for survival (model depicted in Figure 7F). In the cancer metabolism program, the Warburg effect is considered a hallmark of cancer, and the pentose-phosphate pathway and high TCA activity are essential for tumor growth glycolysis (Foster et al., 2012; Garcia-Cao et al., 2012; Lunt and Vander Heiden, 2011; Ying et al., 2012). However, in our model, micro-environmental changes induced by antiangiogenic TKIs are followed by a response similar to that observed in healthy tissues during nutritional stress (Soeters et al., 2012): downregulation of glycolysis

(G) Lack of effect of adding phenformin to B20-4.1.1. TGIs: phenformin: 17%; B20-4.1.1: 61%; combination: 64% ($p = 0.645$). Phenformin-treated animals developed faster growth tumors than vehicle-treated tumors in some occasions (one or two tumors per animal out of six to eight growing lesions), mandating sacrifice even though the average size was lower than 1,000 mm^3, explaining the reduction in average growth size compared to vehicle but earlier termination of the treatment groups. $n > 50$ tumors per group; error bars, SEM.

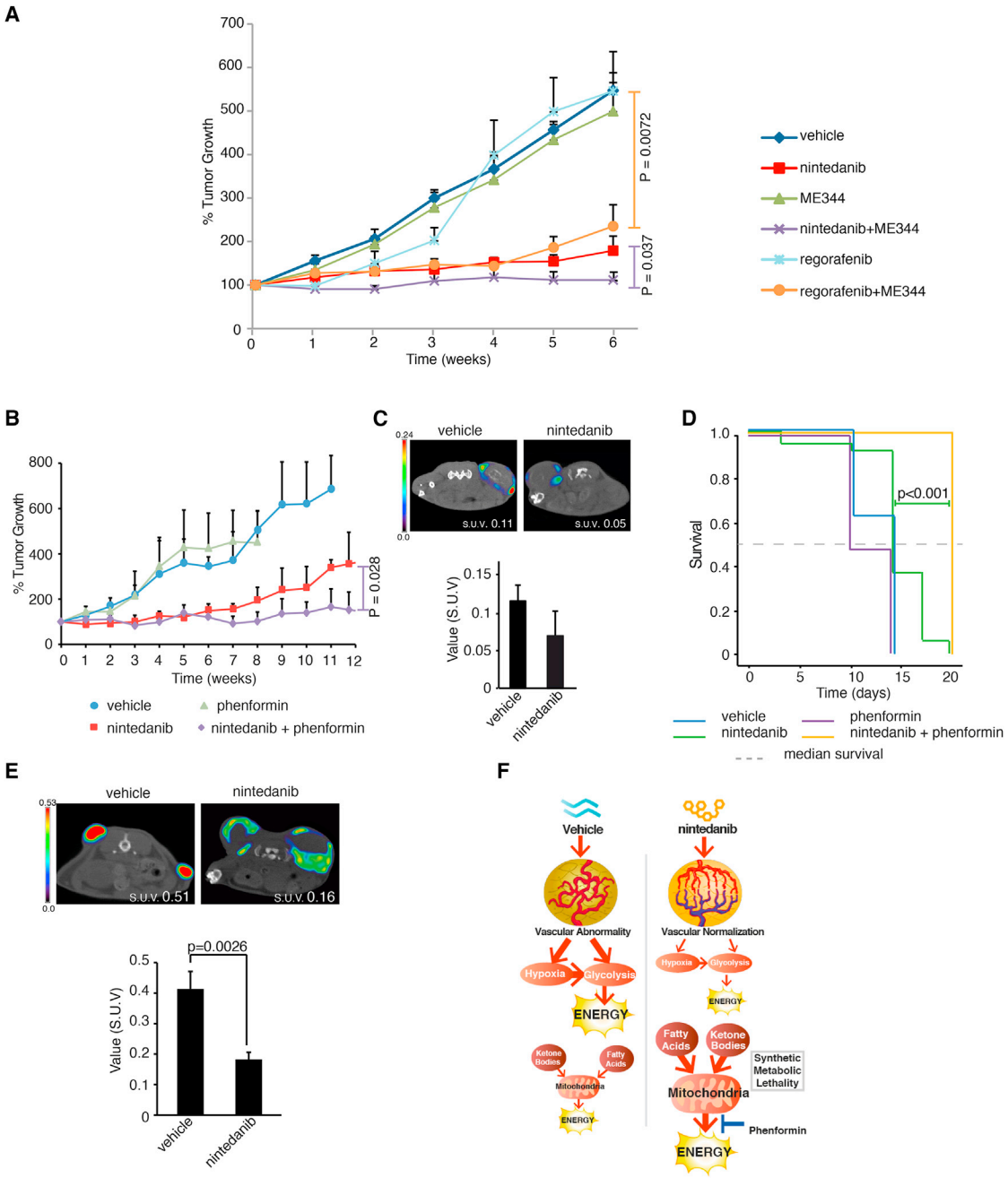

Figure 7. Metabolic Synthetic Lethality Is Observed with Different Agents and Is Extended to Lung Cancer Models

(A) Tumor growth of PyMT tumors treated with vehicle, nintedanib, regorafenib, ME344, or either TKI plus ME344.

(B) TGIs (calculated at T = 8 weeks, T_{end} of phenformin): nintedanib: 58%; phenformin: 10%; nintedanib + phenformin: 80% - synergistic (p = 0.028).

(C) FDG-PET of nintedanib-treated Pulm24 xenografts.

(D) Kaplan-Meier survival plots; p < 0.001 (log-rank) nintedanib versus nintedanib+phenformin; median survival time: 14 versus 20 days.

(E) Tumor glucose uptake by FDG-PET was significantly lower over the long term with nintedanib-treated LLC (−52%, p = 0.0026). n > 50 tumors per group; error bars, SEM.

(F) Schematics of antiangiogenic-induced metabolic changes. Vehicle-treated tumors mainly relied on glycolysis. The antiangiogenic treatment with TKIs normalized the tumor vasculature and decreased hypoxia, decreasing the glycolytic flux. In turn, mitochondrial metabolism increased and sustained tumor growth long term. However, in these conditions, the ability to switch from one metabolic source to another was impaired and rendered the mitochondrial metabolism essential for tumor survival, evidenced by the effects of several mitochondrial metabolism inhibitors in combination with the TKIs.

(mediated through decreased HIF1α and AKT signaling); activation of AMPK, PPARα, and PKA; uptake of ketones and fatty acids from the bloodstream elicited by increased expression of transporters; and upregulation of mitochondrial metabolism. When one energy source (glycolysis) is pharmacologically limited, the tumors become vulnerable to the inhibition of the other (mitochondrial metabolism). Pharmacological blockers of the nutritional stress response (phenformin and ME344) can abrogate mitochondrial respiration and tumor growth in this situation, which we have termed "metabolic synthetic lethality." Priming with antiangiogenic treatment, rather than administering concurrent treatment, shows the most intense therapeutic effects (Figure 6F). Inhibitors of PPARα (GW6471 [Figure S4A]) or PKA activation (propranolol [Figure S4B]) also enhance the TGI effects of the TKIs, which suggests a possible mechanistic link between these two signaling nodes and the adaptive mitochondrial response in this context. Because of the lack of specific inhibitors of ketone bodies degradation, we cannot address the relative contribution of this metabolic source to the metabolic adaptation. The observed metabolic synthetic lethality is completely non-cell autonomous, according to the in vitro data; the ultimate reason for the synthetic lethality in vivo is unclear but likely secondary to the changes induced by the TKI in the levels of oxygen and glucose in the tumor microenvironment.

Study conclusions about angiogenesis in translational oncology have sometimes been contradictory, probably because the investigations rely on different models, therapeutic schemes, drug classes, or agents. Angiogenesis is a complex process, and understanding the mechanisms of resistance with therapeutic purposes depends on the mechanism of action of the specific agent under study and the tumor type. The model used for study may also be a factor. For example, xenograft models differ from spontaneous cancer models in that the former lacks natural tumor growth kinetics or immune system, an important regulator of angiogenesis; interspecies stromal interaction may be a confounding factor as well (Sharpless and Depinho, 2006). In addition, the tumor evolves over time as the balance between pro- and antiangiogenic factors inside the tumor changes, and thus the effect of an antiangiogenic drug may tip that balance in different directions depending on the time point (Jain, 2005). In another study, we have observed that dovitinib induces normoxia in several pancreatic PDXs, but hypoxia in others (Hernandez-Agudo et al., 2016). Along similar lines of thought, there is a study reporting hypoxia in various xenografts that were exposed to nintedanib (Kutluk Cenik et al., 2013), an effect that we reproduced, for example, with the MDA-MB-231 breast cancer cell line (data not shown). This heterogeneity in the type of interstitial response may be caused by a great inherent variability in the concentration of pro- and anti-angiogenic factors in different tumors, causing a unique "angiogenic environment" in each tumor type, or by the affinity and K_M of the drugs for different angiogenic targets. However, at least in a fraction of cases the exposure to antiangiogenic treatment may lead to a decrease in glucose avidity and glycolysis. Similarly to the findings by DePinho and Draetta following KRAS ablation in a KRAS-driven model (Viale et al., 2014), we have described how the tumors can rely long term on mitochondrial respiration in vivo instead of on the Warburg effect. These observations are of applicability in clinical trials; nintedanib, regorafenib, ME344, or phenformin are available drugs for which the maximum tolerated doses are already known. Dose-finding combination phase I trials with drugs with already known maximum tolerated doses and toxicities are relatively simple compared to trials involving combinations of investigational agents. On the basis of our findings, we are designing a phase I clinical trial exploring the safety and efficacy of the combination of nintedanib plus phenformin.

EXPERIMENTAL PROCEDURES

Mouse Models

All animal experiments were approved by the CNIO (Spanish National Cancer Research Centre) Ethics Committee and performed in accordance with the guidelines stated in the International Guiding Principles for Biomedical Research Involving Animals developed by the Council for International Organizations of Medical Sciences. PyMT [FVB/N-Tg(MMTV-PyVT)$^{634Mul/J}$] mice were obtained from W. Muller. C57BL/6JOlaHsd were obtained from the CNIO Animal House. Four- to 6-week-old female athymic nude mice (Hsd: Athymic Nude-Foxn1nu) were purchased from Charles River Laboratories.

Pulm24 PDX was kindly provided by Dr. Manuel Hidalgo. Tumors were implanted subcutaneously in the lower back of Athymic Nude-Foxn1nu, and mouse–mouse passages were performed to obtain the experimental animal cohorts as described previously.

For the syngenic model of LLC, cell suspensions (10^5 cells/100 μl) in 1 × PBS were injected subcutaneously into 8-week-old C57BL/6JOlaHsd mice in both flanks.

Animal Treatments

The treatment allocations were randomly assigned using computer-generated random numbers (http://www.randomization.com/). The researcher performing tumor measurements was blinded to the treatment allocation. Treatment with the different drugs was started at 7 weeks of age. B20-4.1.1 (Genentech) was prepared in 1 × PBS and administered at 5 mg/kg intraperitoneally twice per week. Nintedanib (Boehringer-Ingelheim) and regorafenib (Bayer) were administered at 85 and 10 mg/kg/day, respectively, by oral gavage. Phenformin (Sigma-Aldrich) was administered at 300 mg/kg/day in 5% sucrose in drinking water. ME344 was administered at 50 mg/kg intraperitoneally three times per week. Dovitinib (Novartis) was freshly prepared in pH 2.5 water and administered by oral gavage at 40 mg/kg/day. Tamoxifen (Sigma-Aldrich) was administered daily by oral gavage (1.2 mg/kg/day) in 10% ethanol in sunflower oil.

Tumor Measurements and Treatment Combinations Effects

Tumor dimensions were measured once per week using calipers. Tumor volumes were calculated using the formula $V = (D \times d^2)/2$ mm^3, where D is the largest diameter and d is the shortest diameter; all measurements were in millimeters. All tumors arising in mammary glands were measured in each animal. To calculate TGI, we used the following formula: $TGI = [1 - (T_F/T_0)_A/(T_F/T_0)_V] \times 100$, where T_F is the time point analyzed, T_0 is the initial time, A is the corresponding drug, and V is the vehicle.

For treatment combinations, the thresholds for antagonistic, additive, or synergistic effects were calculated as follows: $T_A = F_a + F_b(1 - F_a)$, where F_a is the relative TGI (from 0 to 1) value at a given time point for the first drug and F_b is the relative TGI value at the same time point for the second drug. Variations within ±15% of the additive threshold are considered to be the result of additive drug interactions; combinations exerting <85% of the predicted additive effect are considered indifferent (and below 70%, antagonistic); combinations exerting >115% of the predicted threshold for additive effect synergistic. The effects of the combinations are calculated at the last time point when the animals belonging to the treatment group that was first terminated because of tumor growth among those compared were alive.

Tumor Processing

Animals were killed in a CO_2 chamber, and tumors were dissected from the front limb mammary fat pad. Depending on the procedure, the tumors were

fixed in 10% formalin solution and embedded in paraffin, snap-frozen in isopentane, or OCT-embedded for cryopreservation (TissueTek; Sakura Finetek). A slide stained with H&E was obtained for every tumor to spatially guide macrodissection or microdissection procedures.

Micro Positron Emission Tomography with [^{18}F]Fluorodeoxyglucose

Mice were anesthetized with a continuous flow of 1%–3% isoflurane/oxygen mixture (2 l/min). The mice were injected into the tail vein with 500 μCi of 18F-FDG in a volume of 0.1 ml. Images were acquired using eXplore Vista PET-CT (GE HC) 45 min after radiotracer injection, starting with the micro-CT scan X-ray tube settings 40 kV and 300 μA; 400 projections were collected in one full rotation of the gantry in approximately 10 min. MicroPET scans were immediately performed at 15 min per bed, 30 min in total, to perform a whole-body study. The microPET images were reconstructed using the three-dimensional ordered subsets expectation-maximization reconstruction algorithm. Regions of interest were drawn over breast tumors and quantitative evaluations were performed using AMIDE software to obtain the standardized uptake values (SUVs). The calculation for SUV is as follows:

$$\mathrm{SUV} = \text{tissue radioactivity concentration}(\mathrm{MBq/ml})/\text{injected dose}\ (\mathrm{MBq})/\text{body weight}(\mathrm{g}).$$

Statistics

The sample size for animal experiments was calculated as in the following example: for tumor growth delay, the continuous variable under study is TGI, and the objective is to test whether one treatment group versus another show TGI. The null hypothesis is that TGI is the same across all treatment groups, and the alternate hypothesis is that TGI is different across groups. Parameters for vehicle-treated animals are known: median time to sacrifice is 46 days, and SD is 10.39 days. With $\alpha = 0.05$ and a power of 80%, and measuring at least one tumor per animal, the minimum number of animals per group to detect at least a 30% variation (or 30% TGI), comparing growth curves by ANOVA test, is 10. Assuming a methodological failure of 10%, we treated 11 animals per group. Similar assumptions were made for other quantitative variables (i.e., PET-SUV). In all cases, the sample size was exceeded by at least 20% to avoid "borderline" interpretations (rule for stopping data collection). No data or outliers were excluded from the analysis, besides animals that were found dead for unknown reasons in the cage during treatment (approximately 1%–2% of the >5,000 animals used). Outliers, defined as more than 2 SDs away from the mean value, were included in all calculations in the high-throughput studies. All experiments were performed a minimum of three times.

Mean values for two-way comparisons were determined using a t test. Multiple comparisons involving more than two groups were performed with statistically significant differences among experimental groups and were assessed by one-way ANOVA with Tamhane's adjustment. All tests were performed using the program IBM SPSS statistics version 19, and $p < 0.05$ was considered significant. All comparisons were two tailed. Parametric tests were chosen because of the high number of tumors and animals per group in all experiments. All data are expressed as means ± SEM, except the metabolomic data (boxplots). Specific statistical methods for metabolomic, phosphoproteomic, and transcriptomic data are reported in Supplemental Experimental Procedures.

Other Procedures

Methods for proteomics, metabolomics, and genomics are included in Supplemental Experimental Procedures. In addition, immunohistochemistry, enzymohistochemistry, immunoblots, confocal microscopy, oxygen-consumption assays, RT-PCR and genotyping (including primers), and plasma determinations (ketone bodies and triglycerides), are described in Supplemental Experimental Procedures as well.

ACCESSION NUMBERS

The accession numbers for the gene expression array data and the mass spectrometry proteomics data reported in this paper are GEO: GSE80778 and PRIDE: PXD004071, respectively.

SUPPLEMENTAL INFORMATION

Supplemental Information includes Supplemental Experimental Procedures, seven figures, three tables, and three data files and can be found with this article online at http://dx.doi.org/10.1016/j.celrep.2016.05.052.

AUTHOR CONTRIBUTIONS

M.Q.-F. designed and interpreted the experiments and data, and wrote the manuscript. N.S.C. helped with the data interpretation. P.N. and M.J.B. performed the majority of the experiments. The rest of the authors contributed to data acquisition, interpretation, and data assembly.

ACKNOWLEDGMENTS

M.Q.-F. is a recipient of the following grants: FIS PI10/0288 and FIS PI13/00430 from the Ministry of Health (Spain), 2010-BECA-RETORNO from the AECC Scientific Foundation, and donations from the Rosae Foundation and Avon España S.A.U. I.Z. is a recipient of La Caixa-CNIO PhD 2011 fellowship. M.Q.-F. received research funds from Boehringer-Ingelheim and Novartis.

Received: November 12, 2015
Revised: March 29, 2016
Accepted: May 12, 2016
Published: June 9, 2016

REFERENCES

Baselga, J., Costa, F., Gomez, H., Hudis, C.A., Rapoport, B., Roche, H., Schwartzberg, L.S., Petrenciuc, O., Shan, M., and Gradishar, W.J. (2013). A phase 3 tRial comparing capecitabinE in combination with SorafenIb or pLacebo for treatment of locally advanced or metastatIc HER2-Negative breast CancEr (the RESILIENCE study): study protocol for a randomized controlled trial. Trials *14*, 228.

Bendell, J.C., Patel, M.R., Infante, J.R., Kurkjian, C.D., Jones, S.F., Pant, S., Burris, H.A., 3rd, Moreno, O., Esquibel, V., Levin, W., and Moore, K.N. (2015). Phase 1, open-label, dose escalation, safety, and pharmacokinetics study of ME-344 as a single agent in patients with refractory solid tumors. Cancer *121*, 1056–1063.

Chung, A.S., Wu, X., Zhuang, G., Ngu, H., Kasman, I., Zhang, J., Vernes, J.M., Jiang, Z., Meng, Y.G., Peale, F.V., et al. (2013). An interleukin-17-mediated paracrine network promotes tumor resistance to anti-angiogenic therapy. Nat. Med. *19*, 1114–1123.

Crown, J.P., Diéras, V., Staroslawska, E., Yardley, D.A., Bachelot, T., Davidson, N., Wildiers, H., Fasching, P.A., Capitain, O., Ramos, M., et al. (2013). Phase III trial of sunitinib in combination with capecitabine versus capecitabine monotherapy for the treatment of patients with pretreated metastatic breast cancer. J. Clin. Oncol. *31*, 2870–2878.

Curtis, C., Shah, S.P., Chin, S.F., Turashvili, G., Rueda, O.M., Dunning, M.J., Speed, D., Lynch, A.G., Samarajiwa, S., Yuan, Y., et al.; METABRIC Group (2012). The genomic and transcriptomic architecture of 2,000 breast tumours reveals novel subgroups. Nature *486*, 346–352.

El-Mir, M.Y., Nogueira, V., Fontaine, E., Avéret, N., Rigoulet, M., and Leverve, X. (2000). Dimethylbiguanide inhibits cell respiration via an indirect effect targeted on the respiratory chain complex I. J. Biol. Chem. *275*, 223–228.

Foster, R., Griffin, S., Grooby, S., Feltell, R., Christopherson, C., Chang, M., Sninsky, J., Kwok, S., and Torrance, C. (2012). Multiple metabolic alterations exist in mutant PI3K cancers, but only glucose is essential as a nutrient source. PLoS ONE *7*, e45061.

Garcia-Cao, I., Song, M.S., Hobbs, R.M., Laurent, G., Giorgi, C., de Boer, V.C., Anastasiou, D., Ito, K., Sasaki, A.T., Rameh, L., et al. (2012). Systemic elevation of PTEN induces a tumor-suppressive metabolic state. Cell *149*, 49–62.

Heist, R.S., Wang, X., Hodgson, L., Otterson, G.A., Stinchcombe, T.E., Gandhi, L., Villalona-Calero, M.A., Watson, P., Vokes, E.E., and Socinski, M.A.; Alliance for Clinical Trials in Oncology (2014). CALGB 30704 (Alliance): A

randomized phase II study to assess the efficacy of pemetrexed or sunitinib or pemetrexed plus sunitinib in the second-line treatment of advanced non-small-cell lung cancer. J. Thorac. Oncol. *9*, 214–221.

Hernandez-Agudo, E., Mondejar, T., Soto-Montenegro, M.L., Megias, D., Mouron, S., Sanchez, J., Hidalgo, M., Lopez-Casas, P.P., Mulero, F., Desco, M., et al. (2016). Monitoring vascular normalization induced by antiangiogenic treatment with F-fluoromisonidazole-PET. Mol. Oncol. *10*, 704–718.

Hsu, C.C., Wang, C.H., Wu, L.C., Hsia, C.Y., Chi, C.W., Yin, P.H., Chang, C.J., Sung, M.T., Wei, Y.H., Lu, S.H., and Lee, H.C. (2013). Mitochondrial dysfunction represses HIF-1α protein synthesis through AMPK activation in human hepatoma HepG2 cells. Biochim. Biophys. Acta *1830*, 4743–4751.

Jain, R.K. (2005). Normalization of tumor vasculature: an emerging concept in antiangiogenic therapy. Science *307*, 58–62.

Jain, R.K. (2013). Normalizing tumor microenvironment to treat cancer: bench to bedside to biomarkers. J. Clin. Oncol. *31*, 2205–2218.

Kandoth, C., McLellan, M.D., Vandin, F., Ye, K., Niu, B., Lu, C., Xie, M., Zhang, Q., McMichael, J.F., Wyczalkowski, M.A., et al. (2013). Mutational landscape and significance across 12 major cancer types. Nature *502*, 333–339.

Kerbel, R.S. (2006). Antiangiogenic therapy: a universal chemosensitization strategy for cancer? Science *312*, 1171–1175.

Kutluk Cenik, B., Ostapoff, K.T., Gerber, D.E., and Brekken, R.A. (2013). BIBF 1120 (nintedanib), a triple angiokinase inhibitor, induces hypoxia but not EMT and blocks progression of preclinical models of lung and pancreatic cancer. Mol. Cancer Ther. *12*, 992–1001.

Li, F., Wang, D., Zhou, Y., Zhou, B., Yang, Y., Chen, H., and Song, J. (2008). Protein kinase A suppresses the differentiation of 3T3-L1 preadipocytes. Cell Res. *18*, 311–323.

Liang, W.C., Wu, X., Peale, F.V., Lee, C.V., Meng, Y.G., Gutierrez, J., Fu, L., Malik, A.K., Gerber, H.P., Ferrara, N., and Fuh, G. (2006). Cross-species vascular endothelial growth factor (VEGF)-blocking antibodies completely inhibit the growth of human tumor xenografts and measure the contribution of stromal VEGF. J. Biol. Chem. *281*, 951–961.

Lu, K.V., Chang, J.P., Parachoniak, C.A., Pandika, M.M., Aghi, M.K., Meyronet, D., Isachenko, N., Fouse, S.D., Phillips, J.J., Cheresh, D.A., et al. (2012). VEGF inhibits tumor cell invasion and mesenchymal transition through a MET/VEGFR2 complex. Cancer Cell *22*, 21–35.

Lunt, S.Y., and Vander Heiden, M.G. (2011). Aerobic glycolysis: meeting the metabolic requirements of cell proliferation. Annu. Rev. Cell Dev. Biol. *27*, 441–464.

Martin, M.J., Hayward, R., Viros, A., and Marais, R. (2012). Metformin accelerates the growth of BRAF V600E-driven melanoma by upregulating VEGF-A. Cancer Discov. *2*, 344–355.

Nisancioglu, M.H., Betsholtz, C., and Genové, G. (2010). The absence of pericytes does not increase the sensitivity of tumor vasculature to vascular endothelial growth factor-A blockade. Cancer Res. *70*, 5109–5115.

Oliner, J., Min, H., Leal, J., Yu, D., Rao, S., You, E., Tang, X., Kim, H., Meyer, S., Han, S.J., et al. (2004). Suppression of angiogenesis and tumor growth by selective inhibition of angiopoietin-2. Cancer Cell *6*, 507–516.

Orecchioni, S., Reggiani, F., Talarico, G., Mancuso, P., Calleri, A., Gregato, G., Labanca, V., Noonan, D.M., Dallaglio, K., Albini, A., and Bertolini, F. (2015). The biguanides metformin and phenformin inhibit angiogenesis, local and metastatic growth of breast cancer by targeting both neoplastic and microenvironment cells. Int. J. Cancer *136*, E534–E544.

Ostergaard, L., Tietze, A., Nielsen, T., Drasbek, K.R., Mouridsen, K., Jespersen, S.N., and Horsman, M.R. (2013). The relationship between tumor blood flow, angiogenesis, tumor hypoxia, and aerobic glycolysis. Cancer Res. *73*, 5618–5624.

Pracharoenwattana, I., Zhou, W., and Smith, S.M. (2010). Fatty acid beta-oxidation in germinating Arabidopsis seeds is supported by peroxisomal hydroxypyruvate reductase when malate dehydrogenase is absent. Plant Mol. Biol. *72*, 101–109.

Quintela-Fandino, M., Urruticoechea, A., Guerra, J., Gil, M., Gonzalez-Martin, A., Marquez, R., Hernandez-Agudo, E., Rodriguez-Martin, C., Gil-Martin, M., Bratos, R., et al. (2014). Phase I clinical trial of nintedanib plus paclitaxel in early HER-2-negative breast cancer (CNIO-BR-01-2010/GEICAM-2010-10 study). Br. J. Cancer *111*, 1060–1064.

Reck, M., Kaiser, R., Mellemgaard, A., Douillard, J.Y., Orlov, S., Krzakowski, M., von Pawel, J., Gottfried, M., Bondarenko, I., Liao, M., et al.; LUME-Lung 1 Study Group (2014). Docetaxel plus nintedanib versus docetaxel plus placebo in patients with previously treated non-small-cell lung cancer (LUME-Lung 1): a phase 3, double-blind, randomised controlled trial. Lancet Oncol. *15*, 143–155.

Scagliotti, G., Novello, S., von Pawel, J., Reck, M., Pereira, J.R., Thomas, M., Abrão Miziara, J.E., Balint, B., De Marinis, F., Keller, A., et al. (2010). Phase III study of carboplatin and paclitaxel alone or with sorafenib in advanced non-small-cell lung cancer. J. Clin. Oncol. *28*, 1835–1842.

Sharpless, N.E., and Depinho, R.A. (2006). The mighty mouse: genetically engineered mouse models in cancer drug development. Nat. Rev. Drug Discov. *5*, 741–754.

Shojaei, F., Wu, X., Malik, A.K., Zhong, C., Baldwin, M.E., Schanz, S., Fuh, G., Gerber, H.P., and Ferrara, N. (2007). Tumor refractoriness to anti-VEGF treatment is mediated by CD11b+Gr1+ myeloid cells. Nat. Biotechnol. *25*, 911–920.

Soeters, M.R., Soeters, P.B., Schooneman, M.G., Houten, S.M., and Romijn, J.A. (2012). Adaptive reciprocity of lipid and glucose metabolism in human short-term starvation. Am. J. Physiol. Endocrinol. Metab. *303*, E1397–E1407.

Taylor, R.W., Barron, M.J., Borthwick, G.M., Gospel, A., Chinnery, P.F., Samuels, D.C., Taylor, G.A., Plusa, S.M., Needham, S.J., Greaves, L.C., et al. (2003). Mitochondrial DNA mutations in human colonic crypt stem cells. J. Clin. Invest. *112*, 1351–1360.

Viale, A., Pettazzoni, P., Lyssiotis, C.A., Ying, H., Sánchez, N., Marchesini, M., Carugo, A., Green, T., Seth, S., Giuliani, V., et al. (2014). Oncogene ablation-resistant pancreatic cancer cells depend on mitochondrial function. Nature *514*, 628–632.

Xu, L., Stevens, J., Hilton, M.B., Seaman, S., Conrads, T.P., Veenstra, T.D., Logsdon, D., Morris, H., Swing, D.A., Patel, N.L., et al. (2014). COX-2 inhibition potentiates antiangiogenic cancer therapy and prevents metastasis in preclinical models. Sci. Transl. Med. *6*, 242ra84.

Ying, H., Kimmelman, A.C., Lyssiotis, C.A., Hua, S., Chu, G.C., Fletcher-Sananikone, E., Locasale, J.W., Son, J., Zhang, H., Coloff, J.L., et al. (2012). Oncogenic Kras maintains pancreatic tumors through regulation of anabolic glucose metabolism. Cell *149*, 656–670.